

# A continuum model reproducing the multiple frequency crossovers in acoustic attenuation in glasses

H. Luo<sup>a</sup>, V. M. Giordano<sup>c</sup>, A. Gravouil<sup>a</sup>, A. Tanguy<sup>a,b</sup>

<sup>a</sup>Univ Lyon, INSA-Lyon, CNRS UMR5259, LaMCoS, F-69621, France

<sup>b</sup>ONERA, University Paris-Saclay, Chemin de la Hunière, BP 80100, 92123 Palaiseau, France

<sup>c</sup>Institut Lumière Matière, UMR 5306 Université Lyon 1-CNRS, F-69622 Villeurbanne Cedex, France

---

## Abstract

Structured metamaterials are at the core of extensive research, promising for thermal and acoustic engineering. However, the computational cost required for correctly simulating large systems imposes to use continuous modeling, able to grasp the physics at play without entering in the atomistic details. Crucially, a correct description needs to describe both the extrinsic interface-induced and the intrinsic atomic scale-originated phonon scattering. This latter becomes considerably important when the metamaterial is made out of a glass, which is intrinsically highly dissipative and with a wave attenuation strongly dependent on frequency and temperature. In amorphous systems, the effective acoustic attenuation triggered by multiple mechanisms is now well characterized and exhibits a nontrivial frequency dependence with a double crossover of power laws. Here we propose a continuum mechanical model for a viscoelastic medium, able to bridge atomic and macroscopic scales in amorphous materials and reproduce well the phonon attenuation from GHz to THz with a  $\omega^2 - \omega^4 - \omega^2$  dependency, including the influence of temperature.

*Keywords:* Acoustic attenuation, Constitutive modeling, Dynamic mechanical analysis, Finite-element simulation, Nanomaterials, Viscoelasticity

---

## 1. Introduction

Heterogeneous architected materials have attracted considerable attention on their potential applications [1]. They are manmade structural materials designed for obtaining *ad hoc* properties, that cannot be generally found in nature. They are generally obtained by engineering the interplay between the shape, the properties and possible association of materials at different scales, either in a random spacial distribution (composite materials) either with the repetition of regular patterns (metamaterials). Depending on their application, the lengthscale of such patterns can span from nanometer to macroscopic range. For example, metamaterials have been initially investigated for applications in

acoustics, for realizing acoustic guides, filters, lenses [2, 3, 4, 5]. And recently, they have also been introduced into the field of thermal science, for realizing tunable multi-functional thermal metamaterials [6, 7], thermal cloaks and camouflage [8], etc. In both applications, it is matter of guiding, filtering, hindering, the propagation of acoustic waves (phonons), responsible for the sound propagation when their wavelength is macroscopic, and for thermal transport at room temperature when it is nanometric.

A heterogeneous architected material affects the propagation of the acoustic waves mainly by introducing an extrinsic source of scattering, represented by the interfaces. In the specific case of metamaterials featuring periodicity, novel coherent effects arise due to the Bragg scattering. As a result, a new Brillouin Zone can be defined, which strongly modifies the phonon band structure by folding the dispersions at its boundaries, thus introducing new optic modes which can scatter the originally acoustic ones. Moreover, the presence of elemental bricks in the micro-structure introduces local resonances with phonons, leading to the aperture of forbidden gaps in the phonon dispersion [2, 3], useful for the realization of acoustic filters and for impacting thermal transport [9]. Recently, it has been proposed to use amorphous materials as building blocks for metamaterials for thermal transport engineering, due to their renowned low thermal conductivity [10, 11, 12, 13, 14, 15, 9]. Nanocomposites made of amorphous and crystalline components promise to strongly reduce thermal transport.

To correctly describe complex structured materials, it is required to model phonon propagation on large scale systems, more apt at representing real materials, where the effect of heterogeneities and interfaces can be properly investigated. Such large systems are out of reach for atomistic simulations and can be realistically modeled only through continuous modeling. However, a correct description of phonon attenuation in heterogeneous architected materials requires to take into account not only the extrinsic scattering sources introduced by the architected micro-structure, but also the intrinsic attenuation in the component materials, especially when these latter are highly dissipative, as it is the case for amorphous materials.

A multiscale approach is therefore needed, able to connect the atomistic scale, where the intrinsic phonon attenuation takes its origin, and the macroscopic scale, where the metamaterial assembly introduces the extrinsic scattering sources. A particularly restrictive requirement is, that such model should be able to reproduce the frequency- and temperature-dependence of the intrinsic acoustic attenuation, which is specific to the microscopic mechanisms at play.

In glasses, apparent acoustic attenuation can be related to a viscous consumption of mechanical energy induced by anharmonic effects [16], or it can result from acoustic scattering in disordered harmonic systems [17, 18, 19, 20]. It can be temperature-dependent, or not [21, 22, 23, 24, 25, 26]. Most interestingly, it is frequency-dependent [22, 27]. Numerous experiments and numerical works (atomistic simulations) have investigated the acoustic attenuation [22, 23, 24, 25, 28, 29, 21, 30, 31, 32, 33, 34, 35, 26, 36, 18, 37, 38, 39]. A non-exhaustive summary of experimental and theoretical literature results on acoustic attenuation in glasses is reported in Tab.1 and SM Tab. S1. Many

attenuation channels are involved, whose importance depends on phonon frequency and temperature: tunneling due to two level systems [40, 41], soft modes [42, 43, 44], thermally activated relaxation processes [27], anharmonicity [16], and scattering resulting from structural disorder [17, 18, 20]. This last contribution is temperature independent, and dominates acoustic attenuation at frequencies in the GHz-THz range [19]. For lower frequencies, anharmonicity gives rise to a phonon attenuation, or damping,  $\Gamma$ , inversely proportional to phonon lifetime, which changes with frequency as  $\omega^a$  with  $a \approx 1.5 - 2$  [26]. Approaching the THz range, corresponding to phonon wavelengths in the nanometer scale, scattering on structural atomistic disorder starts to dominate, characterized by a Rayleigh-like dependence  $\Gamma \propto \omega^4$  [18, 45], with a progressive transition to a strong scattering regime, finally leading to a new high frequency  $\Gamma \propto \omega^2$  regime, as reported in a number of experimental and theoretical studies [23, 24, 46, 47, 25, 22, 48, 27, 49], eventually followed by a sudden drop [19]. The transition to strong scattering takes place at frequencies comparable with the Boson Peak, i.e. the excess of modes in the phonon density of states with respect to the Debye prediction at low frequency, and has been explained as due to phonon scattering by nanometric elastic heterogeneities [50, 51, 45, 48, 49, 52, 53, 54]. At low temperature, molecular-dynamics simulations have been able to reproduce this attenuation crossover, with some different scaling rules [29, 52, 17, 18, 36]. The addition of anharmonicity at finite temperatures has finally provided a complete picture of the combination of the different attenuation channels [46, 26].

On the whole, three regimes of acoustic attenuation versus frequency can be classified : (1)  $\Gamma \propto \omega^a$  due to the anharmonicity at low frequencies, with  $a \approx 1.5 - 2$  and temperature dependent strength; (2)  $\Gamma \propto \omega^4$  due to Rayleigh-like scattering induced by disorder and leading to a dramatic phonon lifetime reduction, so that the collective vibrational modes lose progressively their plane wave character; (3)  $\Gamma \propto \omega^2$  above Ioffe-Regel frequency ( $\omega_{IR} = \pi\Gamma$ ), where phonons cannot be considered as propagative plane waves anymore. As such, they do not propagate anymore but are diffusive, and, at higher frequency, even may localize (in the Anderson's definition of localization, but for acoustic waves) [55, 17, 20, 56, 57].

Nevertheless, little consideration has been given so far to the use of those results on acoustic attenuation at the macroscale due to the lack of adapted continuum constitutive laws. A continuous model is expected to describe the effective mechanical behavior without knowing the atomistic details. However, the peculiar frequency and temperature dependence of attenuation in glasses needs to be somehow reproduced in order to have realistic macroscale dynamical simulations of acoustic properties for large structures or composites. In this context, we thus need to connect atomistic and macroscopic scale, keeping the information on the active intrinsic attenuation channels and the microscopic frequency and temperature dependence of phonon attenuation.

To do so, a model is urgently needed to homogenize the effective attenuation triggered by multiple mechanisms, and characterized by a defined frequency dependence. Within Stoke's theory [58], the amplitude of a plane wave decreases

Table 1: Experimental results of sound attenuation of glasses in the literature. (TJ: tunneling junction; BLS: Brillouin light scattering; BUVS : Brillouin ultraviolet light scattering; POT: picosecond optical technique.)

| Materials  | Method | T (K)      | Power | Frequency range and/or $\nu_c$         | LA velocity (m/s) | Ref  |
|--|--------|------------|-------|--|-------------------|------|
| v-SiO <sub>2</sub>   | TJ     | 1          | 4     | 0.1-0.4 THz                            |                   | [34] |
|  | BUVS   | 300        | 2     | 5-70 GHz*                              |                   | [31] |
|  | IUVS   | 300        | 2     | 75-95 GHz*                             |                   | [30] |
|  | IUVS   | 300        | 2-4   | 75-150 GHz<br>$\nu_c = 100 \pm 10$ GHz | 5950              | [32] |
|  | POT    | 300        | 2     | near 250 GHz                           | 5940              | [33] |
|  | IXS    | 1050       | 2     | 1-3 THz                                | 5800              | [39] |
|  | IXS    | 1620       | 4-2   | 1- 4THz<br>$\nu_c = 1.5$ THz           | 6500              | [22] |
| d-SiO <sub>2</sub>   | IXS    | 565        | 4.21  | 1.2-1.9 THz                            |                   | [23] |
| Li <sub>2</sub> O-2 <sub>2</sub> B <sub>2</sub> O <sub>3</sub> | BLS    | 300<br>573 | 1     | 20-40 GHz                              | 7600              | [24] |
|  | IXS    | 573        | 4     | 1.2-2.4 THz                            |                   | [24] |
| Glycerol   | IXS    | 16<br>167  | 2     | 0.6-3.5 THz †                          |                   | [21] |
|  | IXS    | 150.1      | 4-2   | 1-2.5 THz<br>$\nu_c = 1.2$ THz         | 3630              | [25] |
| BeF <sub>2</sub>   | IXS    | 297        | 2     | 0.6-6 THz                              | 5500              | [37] |
|  |        |            |       |  |                   | [35] |
| Poly butadiene   | IXS    | 140        | 2     | 0.6-3.6 THz                            | 2770              | [38] |
|  |        |            |       |  |                   | [35] |

\* Use the sound speed value in Ref.[32].

† Use the sound speed value in Ref.[25].

exponentially with the propagation distance in viscous media, with a decay rate given, in the low frequency limit  $\omega\tau \ll 1$ , by  $\gamma = \frac{\omega^2\tau}{2c}$ , with  $\tau = \frac{4\eta}{3\rho c^2}$  where  $\eta$  is the dynamic viscosity coefficient,  $\rho$  is the fluid density and  $c$  is the speed of sound in the absence of viscosity. This behavior leads to a typical attenuation distance  $l = 1/\gamma$  scaling as  $\propto \omega^{-2}$ . A similar exponential attenuation of acoustic wave packets, eventually with another frequency dependence, was also evidenced in amorphous materials up to the Ioffe-Regel frequency [20], allowing defining a mean-free path from the corresponding Beer-Lambert law for acoustic transport attenuation. This behavior is thus similar in amorphous materials and in Newtonian liquids. Glasses could be then characterized by an effective viscoelastic behaviour for their acoustic properties, even below the glass transition temperature (that is, in the solid state). This corresponds to the requirement that the internal friction in the material can be characterized by the quality factor  $Q^{-1} = G''/G'$  where  $G = G' + iG''$  is the complex elastic modulus in the linear regime [40]. This is indeed the case in a glass [19] for frequencies up to the Ioffe-Regel crossover, where acoustic phonons (named propagons [55]) still maintain well-defined wave vectors and whose amplitude exhibits an exponential decay. A relation has been proposed between the microscopic quantity (phonon attenuation) and the macroscopic one (quality factor):  $\Gamma/\omega = Q^{-1}$  [59, 19, 60, 53, 61, 62] able to interpret experimental neutron-scattering data for example, within the Damped Harmonic Oscillator Model for phonons [63].

Recently, we have proved that the above concept can describe acoustic attenuation in an amorphous material at THz frequencies, in a limited range below the Ioffe-Regel criterium[64]. In that work, we have assumed a constant viscosity, thus leading to a  $\omega^2$  behaviour in the acoustic attenuation. However, at such energies, the dominant scattering source is the structural disorder at the atomic scale [49, 19] thus leading to a  $\omega^4$  behaviour, as found in [24, 25, 22, 27, 49, 26]. The corresponding low scattering is potentially responsible for the unusual temperature dependence  $\kappa \propto T$  observed in the low temperature regime [15], while this low temperature sensitivity was also related to anharmonic effects in the 2-level model [40, 42]. The progressive transition to a stronger scattering and to the resulting diffusive motion of initial plane waves will be responsible for the progressive saturation which may be observed as a plateau in the glassy thermal conductivity at around 10 K followed by an increase of  $\kappa$  with the temperature, and is also responsible for the peak in the specific heat at the same temperature [65, 66, 15]. Modeling amorphous materials for thermal applications clearly needs including different frequency dependences, with at least three successive regimes including  $\Gamma \propto \omega^a$  with  $a \approx 2$  to take account of possible anharmonic effects in the low frequency range (low temperatures [26]),  $\Gamma \propto \omega^4$  in the low scattering regime and then  $\Gamma \propto \omega^2$  again at very high frequencies in the strong scattering (diffusive) regime.

In this work, we develop a new continuum mechanical model for a viscoelastic medium, where no disorder is introduced, by taking into account the different attenuation regimes acting in parallel in the rheological responses of glasses. We will show that our model is able to reproduce the attenuation at a macroscopic

level, through a single continuum model, involving the combined effect of parallel sources of acoustic attenuation and their crossovers. By tuning the parameters of the model, our constitutive law can reproduce qualitatively and quantitatively the three regimes of acoustic attenuation versus frequency: successively  $\Gamma \propto \omega^a, \omega^4, \omega^2$  with  $a \approx 2$ .

## 2. Model

Let's assume an isotropic, homogeneous and viscous solid (amorphous materials being homogeneous and isotropic above the nanometer scales [67]): we can express the elastic constitutive laws describing the stress-strain relation using the Hooke's law and separating the hydrostatic from the deviatoric components

$$\sigma_{ij} = 3K\epsilon_{ij}^{sph} + 2G\epsilon_{ij}^{dev} \quad (1)$$

where  $K$  is the generalized bulk modulus and  $G$  is the generalized shear modulus. The hydrostatic (or spherical) part of strain is given by  $\epsilon_{ij}^{sph} = \frac{1}{3}\delta_{ij}\epsilon_{kk}$  and the deviatoric part, which is isochoric, is  $\epsilon_{ij}^{dev} = \epsilon_{ij} - \frac{1}{3}\delta_{ij}\epsilon_{kk}$ , where  $\delta_{ij}$  is Dirac function.

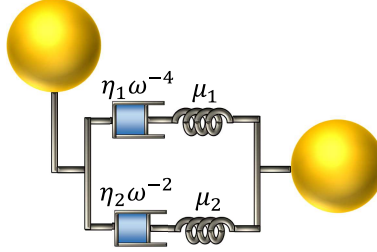


Figure 1: Illustration of the viscoelastic model: two Maxwell-like models in parallel.

In Ref.[64], we proposed to use two different simple rheological models for the spherical and deviatoric parts separately, determining the longitudinal and transverse quality factor. Here, we propose a new model for the transverse modes. As shown in Fig. 1, we assume two Maxwell-like models in parallel, with  $\mu_1$  and  $\mu_2$  the rigidity and  $\eta_1\omega^{-4}$  and  $\eta_2\omega^{-2}$  the frequency-dependent viscosity, respectively. The physical idea behind this model is the asynchronous activation of the  $\omega^4$  and the  $\omega^2$  dependence of the attenuation, resulting from two processes contributing additionally to the global stress in the system. The frequency-dependent elastic modulus  $G^*(\omega) = G'(\omega) + iG''(\omega)$  for the model illustrated in Fig. 1 can be expressed as:

$$G^*(\omega) = \frac{i\mu_1\eta_1\omega^{-3}}{i\eta_1\omega^{-3} + \mu_1} + \frac{i\mu_2\eta_2\omega^{-1}}{i\eta_2\omega^{-1} + \mu_2} \quad (2)$$

We can write down the full complex constitutive elastic tensor  $\mathbb{G}^*$  [64], which is reduced to a  $6 \times 6$  symmetric matrix due to isotropy, imposing the conditions

$G_{11}^* = G_{22}^* = G_{33}^* = K^*(\omega) + \frac{2}{3}G^*(\omega)$  and  $G_{44}^* = G_{55}^* = G_{66}^* = G^*(\omega)$ , being directly related to sound propagation and attenuation. By definition, isotropic longitudinal (L) and transverse (T) sound speeds are defined as

$$\begin{cases} v_L(\omega)^2 &= \frac{G'_{11}(\omega)}{\rho} \\ v_T(\omega)^2 &= \frac{G'_{44}(\omega)}{\rho} \end{cases} \quad (3)$$

similarly, the inverse quality factors are obtained as:

$$Q_L^{-1}(\omega) = \frac{G''_{11}(\omega)}{G'_{11}(\omega)} \quad \text{and} \quad Q_T^{-1}(\omega) = \frac{G''_{44}(\omega)}{G'_{44}(\omega)} \quad (4)$$

where  $G'_{ij} = \text{Re}(G_{ij}^*)$  and  $G''_{ij} = \text{Im}(G_{ij}^*)$ .

We will derive the complex elastic modulus in order to obtain the analytic expression of the quality factor  $Q^{-1} = G''/G'$ . Holding the relation  $Q^{-1} = \Gamma/\omega$ , ideally, we expect to get a  $\omega^3-\omega^1-\omega^3$  behavior for  $Q^{-1}$ . At the same time, the amplitude of  $\Gamma/\omega$  and the crossover position should be clearly reproduced.

From Eq.2,  $G'$  and  $G''$  can be extracted:

$$\begin{aligned} G'(\omega) &= \frac{\mu_1 \eta_1^2}{\mu_1^2 \omega^6 + \eta_1^2} + \frac{\mu_2 \eta_2^2}{\mu_2^2 \omega^2 + \eta_2^2} \\ &= \mu_1 \left( \frac{\tau_1^2}{\omega^6 + \tau_1^2} + \alpha \frac{\tau_2^2}{\omega^2 + \tau_2^2} \right) \end{aligned} \quad (5)$$

$$\begin{aligned} G''(\omega) &= \frac{\mu_1^2 \eta_1 \omega^3}{\mu_1^2 \omega^6 + \eta_1^2} + \frac{\mu_2^2 \eta_2 \omega}{\mu_2^2 \omega^2 + \eta_2^2} \\ &= \mu_1 \left( \frac{\tau_1 \omega^3}{\omega^6 + \tau_1^2} + \alpha \frac{\tau_2 \omega}{\omega^2 + \tau_2^2} \right) \end{aligned} \quad (6)$$

where  $\tau_1 = \frac{\eta_1}{\mu_1} (\text{s}^{-3})$ ,  $\tau_2 = \frac{\eta_2}{\mu_2} (\text{s}^{-1})$  and  $\alpha = \frac{\mu_2}{\mu_1}$ . As such, there are only three parameters left to characterize the attenuation. Finally, the quality factor  $Q^{-1} = G''/G'$  is given by:

$$\begin{aligned} Q^{-1}(\omega) &= \frac{\frac{\tau_1 \omega^3}{\omega^6 + \tau_1^2} + \alpha \frac{\tau_2 \omega}{\omega^2 + \tau_2^2}}{\frac{\tau_1^2}{\omega^6 + \tau_1^2} + \alpha \frac{\tau_2^2}{\omega^2 + \tau_2^2}} \\ &= \frac{\alpha \tau_2 \omega^7 + \tau_1 \omega^5 + \tau_1 \tau_2^2 \omega^3 + \alpha \tau_1^2 \tau_2 \omega}{\alpha \tau_2^2 \omega^6 + \tau_1^2 \omega^2 + (1 + \alpha) \tau_1^2 \tau_2^2} \end{aligned} \quad (7)$$

As discussed in the SM Appendix, we show the existence of  $\omega-\omega^3-\omega$  behavior given by the quality factor  $Q^{-1}$  of our model, indicating that the model is capable to describe  $\Gamma \propto \omega^2-\omega^4-\omega^2$  energy-dependent attenuation.

### 3. Results

In order to use our model, we need to calibrate it against attenuation results from microscopic experimental or theoretical results. Similarly to what we have done in Ref.[68], we calibrate our model on literature data on the prototype glass SiO<sub>2</sub>. Reported attenuations are for longitudinal modes only, but it has been demonstrated that the same phenomenology is present in transverse modes at higher values of  $q$  and  $\omega$ , making the computations more comfortable [26]. The experimental results of SiO<sub>2</sub> are reported in Fig. 2 in which sound attenuation  $\Gamma$  is measured at 300K in the subterahertz range ( $\nu < 0.3$  THz with  $\omega = 2\pi\nu$ ) and at 1620K at terahertz frequencies ( $\nu > 1$  THz). The three regimes mentioned before can be clearly found in the figures. At high frequency, a  $\omega^4$ - $\omega^2$  crossover of  $\Gamma$  appears around  $\omega = 1 \times 10^{13}$  rad  $\cdot$  s<sup>-1</sup> ( $\nu = 1.5$  THz) as shown in Fig. 2. In addition, in the subterahertz range, there should be another  $\omega^2$ - $\omega^4$  crossover which is not explicitly given by the experimental data but shown as the intersection of the auxiliary lines ( $\omega^2$  and  $\omega^4$ ). By adjusting the parameters of the model ( $\tau_1$ ,  $\tau_2$  and  $\alpha$ ), we give our best fit in Fig. 2 for high (red line) and low (green line) temperature. The fitting parameters for high temperature are reported in Tab. 2. The results of the fit at high temperature is excellent. As for the low temperature data, it would be extremely interesting to compare with data in the 0.1-10 THz range. Unfortunately, no data in this range at low temperature are available in literature.

Table 2: Parameters of the new viscoelastic continuum model. Calibration on silica glass at high temperature [27, 22].

| $\tau_1(\text{s}^{-3})$ | $\tau_2(\text{s}^{-1})$ | $\alpha$ |
|-------------------------|-------------------------|----------|
| $3 \times 10^{39}$      | $2.7 \times 10^{13}$    | 1.4      |

It is worth going more in the detail of the fitting procedure to highlight the role of each parameter. A good fit should give a  $Q^{-1}$  reproducing not only the amplitude of the acoustic attenuation, but also at least the crossover from  $\omega^4$  to  $\omega^2$  around  $1 \times 10^{13}$  rad  $\times$  s<sup>-1</sup> ( $\nu = \omega/2\pi = 1.5$  THz). It is not easy to reach these two conditions through a simple optimization algorithm, because most of the time it only meets the amplitude condition but the crossover condition is ignored. To meet the two conditions simultaneously, we start with a know-how to illustrate the evolution of the amplitude and the crossover frequencies versus the three parameters  $\tau_1$ ,  $\tau_2$  and  $\alpha$ . This approach is necessary as the first step of the parameters identification before finding an alternative optimization algorithm in future work.

The roles of the three parameters are displayed one by one in Fig. 3. By default, we set  $\tau_1 = 10^{30}$  s<sup>-3</sup>,  $\tau_2 = 10^{10}$  s<sup>-1</sup> and  $\alpha = 1$ . The chosen order of magnitude for different parameters can be estimated based on the crossover positions.

Let's first consider  $\tau_2$ , as shown in the left panel of Fig. 3. We can find that the global amplitude of the  $Q^{-1}$  decreases with  $\tau_2$ . Therefore, in the first step, we change  $\tau_2$  in order to get the same order of magnitude for  $Q^{-1}$  obtained in

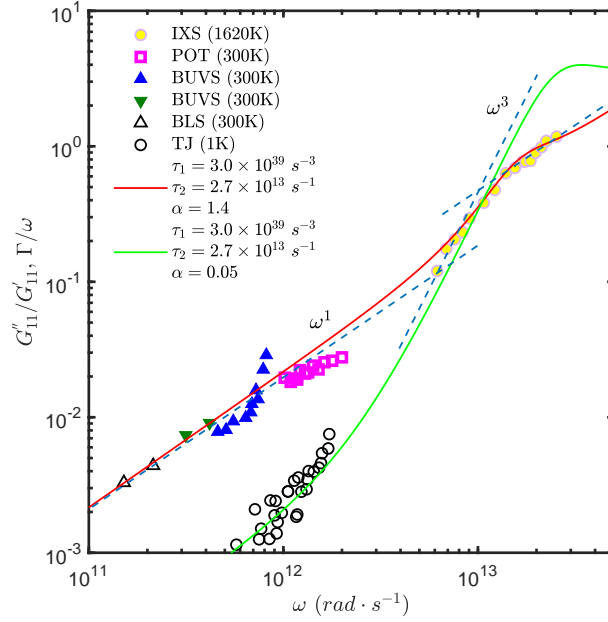


Figure 2: Comparison between  $\Gamma/\omega$  and  $Q^{-1}$  with  $\tau_1 = 3 \times 10^{39} \text{s}^{-3}$ ,  $\tau_2 = 2.7 \times 10^{13} \text{s}^{-1}$  and  $\alpha = 1.4$  (red line) or  $\alpha = 0.05$  (green line). The red (green) line is the  $Q^{-1}$  of the present viscoelastic model. Experimental data are from: IXS [22], POT [27], BUVS [32, 31], BLS [69] and TJ [34]. The blue dashed lines are two power-law fits representing  $\Gamma/\omega \propto \omega$  and  $\Gamma/\omega \propto \omega^3$ , respectively.

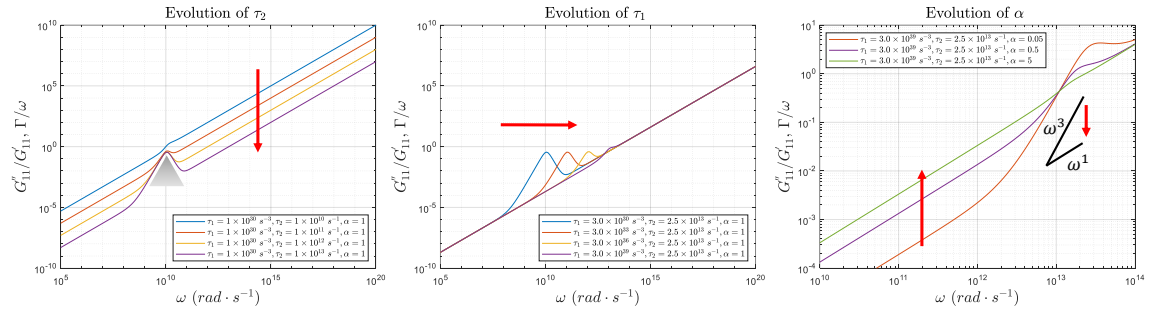


Figure 3: Evolution of  $Q^{-1}$  as a function of  $\tau_2$ ,  $\tau_1$  and  $\alpha$ , respectively. The red arrow indicates the growth direction of the parameter.

Table 3: Estimation of the relaxation time for  $\tau_1 = 3 \times 10^{39} \text{ s}^{-3}$  and  $\tau_2 = 2.7 \times 10^{13} \text{ s}^{-1}$ .

| $\omega$ (rad · s <sup>-1</sup> ) | $\tau_1 \omega^{-4}$ (s) | $\tau_2 \omega^{-2}$ (s) |
|-----------------------------------|--------------------------|--------------------------|
| $1 \times 10^{11}$                | $3 \times 10^{-5}$       | $2.7 \times 10^{-9}$     |
| $1 \times 10^{12}$                | $3 \times 10^{-9}$       | $2.7 \times 10^{-11}$    |
| $1 \times 10^{13}$                | $3 \times 10^{-13}$      | $2.7 \times 10^{-13}$    |
| $3 \times 10^{13}$                | $3.7 \times 10^{-15}$    | $3 \times 10^{-14}$      |

the numerical model, and the experimental values of  $\Gamma/\omega$ . During this process, one peak appears at  $\omega = 1 \times 10^{10} \text{ rad} \cdot \text{s}^{-1}$  whose position and amplitude are determined by the two other parameters. This peak corresponds to a transition between two different dominant frequency powers in the constitutive model and depends on the relation among three parameters of the model. In the current configuration, that is for  $\tau_1 = 1 \times 10^{30} \text{ s}^{-3}$  and  $\alpha = 1$ , it shows a  $\omega^3 - \omega^{-3}$  crossover.

Let's now consider the variations of  $\tau_1$ , after having optimized  $\tau_2$ . The influence of  $\tau_1$  is shown in the middle panel of Fig. 3. Increasing  $\tau_1$  pushes to the right the above  $\omega^3 - \omega^{-3}$  peak. When this peak moves to the right, it becomes smaller and the  $\omega^{-3}$  part disappears first due to the collapse with the increasing  $\omega$  background. In this step, only the peak moves and the amplitude of left or right wing is unchanged.

Finally, let's consider the role played by the ratio  $\alpha = \mu_1/\mu_2$ , which characterizes the rigidity ratio between the two parallel processes of dissipation contributing additionally to the stress state. As shown in the right panel of Fig. 3, changing  $\alpha$  will raise or lower the left wing and modify the power law near the crossover between left and right wing. When  $\alpha \ll 1$ , the left wing will drop significantly. However, when  $\alpha \gg 1$ , the crossover  $\omega^3 - \omega^{-3}$  will progressively disappear and the whole line, especially the part  $\propto \omega^3$ , tends to a single  $\omega$  power law. Between them, the  $\omega^3$  tends to  $\omega$ . Therefore, an appropriate  $\alpha$  should raise the left wing to fit the experiments data, while keeping the  $\omega^3$  apparent power law as much as possible.

In addition, the relaxation times  $\tau_1 \omega^{-4}$  and  $\tau_2 \omega^{-2}$  should make sense physically, which requires them being longer than  $1 \times 10^{-14} - 1 \times 10^{-15} \text{ s}$ . Using the orders of magnitude of  $\tau_1$  and  $\tau_2$ , we estimate the corresponding relaxation time in Tab.3. Relaxation times shorten as the frequency increases, indicating as upper frequency limit for this model  $3 \times 10^{13} \text{ Hz}$ , that is satisfactory.

In SM Appendix, we discuss in more details the conditions giving rise to a  $\omega - \omega^3 - \omega$  behavior. If these conditions are strictly met, then the crossover frequencies can be expressed in terms of  $\alpha$ ,  $\tau_1$  and  $\tau_2$ . We recall the two crossover frequencies evidenced in SM Appendix:

- Position of the crossover  $\omega - \omega^3$ :

$$\omega_{1-3} = \frac{1}{\alpha + 1} \tau_2$$

- Position of the crossover  $\omega^3 - \omega$ :

$$\omega_{3-1} = \left(\frac{1}{\alpha}\right)^{1/2} \left(\frac{1}{\alpha+1}\right)^{1/2} \tau_2$$

Note that in the present model, the ratio  $\omega_{3-1}/\omega_{1-3}$  depends only on  $\alpha$ . It is given by :

$$\frac{\omega_{3-1}}{\omega_{1-3}} = \sqrt{\frac{\alpha+1}{\alpha}} \quad (8)$$

where  $\alpha > 0.76$  is a necessary condition to have a perfect  $\omega - \omega^3 - \omega$  behavior without exhibiting other power laws (this condition disappears if other crossovers are allowed). This gives an upper limit of the ratio  $\omega_{3-1}/\omega_{1-3}$  less than 1.52. In practice, these conditions may not be strictly met but were sufficient in our case. Moreover, the results about the crossover frequencies are still very useful because they determine the magnitude of the parameters. For example, knowing that  $\omega_{3-1} \approx 2\pi \times 1.5 \text{ THz} \approx 9.4 \times 10^{12} \text{ rad} \cdot \text{s}^{-1}$  and  $\alpha$  is normally supposed as 1 at first, then we have  $\tau_2 = \omega_{3-1}/\sqrt{0.5} \approx 1.3 \times 10^{13} \text{ s}^{-1}$  and  $\tau_1 = \frac{\tau_2^3}{4} \approx 5 \times 10^{38} \text{ s}^{-3}$ .

#### 4. Discussion and Conclusion

Provided the parameters  $\tau_1$ ,  $\tau_2$  and  $\alpha$ , the interesting case with three principal frequency dependencies  $\omega - \omega^3 - \omega$  is only a special case offered by the viscoelastic model. For this special case, we can write down the asymptotic approximation for the three frequency dependencies : (1) Low frequency:  $Q_{(1)}^{-1} \sim \frac{\alpha}{1+\alpha} \frac{1}{\tau_2} \omega$ ; (2) Intermediate frequency:  $Q_{(2)}^{-1} \sim \frac{1}{1+\alpha} \frac{1}{\tau_1} \omega^3$ ; (3) High frequency:  $Q_{(3)}^{-1} \sim \frac{1}{\tau_2} \omega$ . It is noticed that the process with viscosity  $\eta_2 \omega^{-2}$  dominates the low and high frequency regimes, while the  $\eta_1 \omega^{-4}$  process activates mainly in the intermediate frequencies corresponding to the Rayleigh-like damping below the Ioffe-Regel frequency. Especially, it can be seen that, when  $\alpha \gg 1$ ,  $Q_{(1)}^{-1}$  tends to  $\frac{1}{\tau_2} \omega$ , thus  $Q_{(3)}^{-1}$ , and the intermediate regime disappears  $Q_{(2)}^{-1} \sim 0$  as illustrated in Fig.3. In contrast, when  $\alpha \ll 1$ , low-frequency  $\omega$  process gives a smaller value of the quality factor compared to the high-frequency ones. This  $\alpha$ -dependent  $\omega$  process is impressively adapted to describe the temperature-dependent acoustic attenuation  $\Gamma/\omega \propto \omega$  at low frequencies (see Fig.2). This low frequency behavior is known to be due to anharmonicity, thermal activation, often described with the help of two level systems and is also shown in the MD simulations [26]. As such, small  $\alpha$  corresponds to low temperature and large  $\alpha$  corresponds to a relatively high temperature, meaning that the effective role of the temperature would be to soften the  $\eta_2 \omega^{-2}$  process by decreasing its related rigidity  $\mu_2$ . Moreover, our model predicts an extension of the  $\omega^3$  regime at high frequencies in the low temperature case as can be seen in Fig.2 and possibly additional frequency dependencies at higher frequencies difficult to reach experimentally.

As shown in the Tab.3, the frequency-dependent relaxation times given by the fitted values of three parameters are reasonable up to  $\omega = 30 \times 10^{12} \text{ rad} \cdot \text{s}^{-1}$

which covers all spectral range of experimental data. Therefore, we can conclude that the values of this model are physically meaningful.

In conclusion, the model presented here which involves two parallel sources of dissipation with a frequency dependent viscosity is shown able to reproduce the successive attenuation regimes  $\omega^2$  -  $\omega^4$  -  $\omega^2$  observed in glasses. In practice, we investigated a calibration of the model on a-SiO<sub>2</sub> which gives a quality factor  $Q^{-1}$  that fits very well the experimental attenuation data  $\Gamma/\omega$  [22, 23, 21, 30, 31, 32, 33, 34, 39]. Interestingly, the frequency dependence of the viscosities involves two mechanisms: one is related to an attenuation time  $\tau_1\omega^{-4}$  (possibly related to low acoustic scattering at the atomic scale as discussed before [18]), while another involves a relaxation time  $\tau_2\omega^{-2}$  (possibly related to anharmonicity or to strong acoustic scattering at small scale, as already discussed in the introduction). The permanent combination of these two well-known atomistic processes in parallel allows to reproduce the two experimentally observed crossovers in the frequency dependence of the attenuation. The comparison of our model with experimental data on a large frequency range leads to the determination of the 3 parameters involved in the model, that is :  $\tau_1 = 3 \times 10^{39} \text{ s}^{-3}$ ,  $\tau_2 = 2.7 \times 10^{13} \text{ s}^{-1}$  and  $\alpha = 1.4$  at ambient temperature (300K) but was also able to reproduce the temperature dependence in the low frequency part, by tuning only the parameter  $\alpha$  ( $\alpha$  is lowered to 0.05 at 1 K). These numerical values are reasonable for  $\omega < 3 \times 10^{13} \text{ rad} \cdot \text{s}^{-1}$  that is the largest frequency that can be reached at the atomic scale. Thus, our results on the one hand give a description of the effective frequency-dependent acoustic attenuation in SiO<sub>2</sub> glasses ranging from GHz to THz range, and on the other hand consolidate the possibility of homogenizing the multi-channel intrinsic acoustic attenuation from nanometric to macroscopic scales with appropriate viscoelastic models. As such, this model will allow for improved and more realistic large scale simulations of metamaterials with an amorphous component. As an example, in a recent work, we have used continuum finite element modeling to investigate the acoustic attenuation in nanocomposites, which has allowed us to study the effect of the interface scattering on the real size materials, underlining the existence of propagative, diffusive and localized regime, depending on the nanostructure lengthscale and elastic mismatch between the components. Still, in that work no intrinsic acoustic attenuation was considered, the component materials being non-dissipative [68]. The introduction of the dissipation in the amorphous matrix would allow to evidence the competition between extrinsic and intrinsic scattering sources, and to predict the efficiency of the nanostructure in attenuating phonons in a medium where attenuation is already important. Of course, we expect to be confronted to different regimes, depending on phonon frequency: a key role of the extrinsic source for low intrinsic scattering, and a less important effect in the strong scattering regime.

Finally, our model paves the way to further studies, investigating other power laws for phonon attenuation, introducing anisotropy and studying the effect of temperature, allowing to describe thermal transport as well as sound propagation in structured materials of arbitrary complexity.

## Acknowledgement

This work benefited from the early participation of Robin Rouzaud. Interesting discussions with Giulio Monaco are acknowledged. H.L. is financed by the french ministry of research. A.T., H.L. and A.G. thank ECOS chile - grant No. C17E02 for their support.

## References

- [1] O. Bouaziz, Y. Bréchet, and J.D. Embury. Heterogeneous and architected materials: A possible strategy for design of structural materials. *Advanced Engineering Materials*, 10(1-2):24–36, feb 2008.
- [2] Z. Liu. Locally resonant sonic materials. *Science*, 289(5485):1734–1736, sep 2000.
- [3] A. Khelif, B. Aoubiza, S. Mohammadi, A. Adibi, and V. Laude. Complete band gaps in two-dimensional phononic crystal slabs. *Physical Review E*, 74(4):046610, oct 2006.
- [4] Shu Zhang, Leilei Yin, and Nicholas Fang. Focusing ultrasound with an acoustic metamaterial network. *Physical Review Letters*, 102(19):194301, may 2009.
- [5] Steven A. Cummer, Johan Christensen, and Andrea Alù. Controlling sound with acoustic metamaterials. *Nature Reviews Materials*, 1(3):1–13, feb 2016.
- [6] Seungwoo Lee, Byungsoo Kang, Hohyun Keum, Numair Ahmed, John A. Rogers, Placid M. Ferreira, Seok Kim, and Bumki Min. Heterogeneously assembled metamaterials and metadevices via 3d modular transfer printing. *Scientific Reports*, 6(1):1–11, jun 2016.
- [7] Gwanwoo Park, Sunggu Kang, Howon Lee, and Wonjoon Choi. Tunable multifunctional thermal metamaterials: Manipulation of local heat flux via assembly of unit-cell thermal shifters. *Scientific Reports*, 7(1):1–15, jan 2017.
- [8] Sophia R Sklan and Baowen Li. Thermal metamaterials: functions and prospects. *National Science Review*, 5(2):138–141, jan 2018.
- [9] Mahmoud I. Hussein, Chia-Nien Tsai, and Hossein Honarvar. Thermal conductivity reduction in a nanophononic metamaterial versus a nanophononic crystal: A review and comparative analysis. *Advanced Functional Materials*, 30(8):1906718, nov 2019.
- [10] Konstantinos Termentzidis, Patrice Chantrenne, and Pawel Koblinski. Nonequilibrium molecular dynamics simulation of the in-plane thermal conductivity of superlattices with rough interfaces. *Physical Review B*, 79(21):214307, jun 2009.

- [11] Samy Merabia and Konstantinos Termentzidis. Thermal conductance at the interface between crystals using equilibrium and nonequilibrium molecular dynamics. *Physical Review B*, 86(9):094303, sep 2012.
- [12] Arthur France-Lanord, Samy Merabia, Tristan Albaret, David Lacroix, and Konstantinos Termentzidis. Thermal properties of amorphous/crystalline silicon superlattices. *Journal of Physics: Condensed Matter*, 26(35):355801, 2014.
- [13] Maxime Verdier, David Lacroix, Stanislav Didenko, Jean-François Robillard, Evelyne Lampin, Thierno-Moussa Bah, and Konstantinos Termentzidis. Influence of amorphous layers on the thermal conductivity of phononic crystals. *Physical Review B*, 97(11):115435, mar 2018.
- [14] Taishan Zhu, Krishnan Swaminathan-Gopalan, Kevin J. Cruse, Kelly Stephani, and Elif Ertekin. Vibrational energy transport in hybrid ordered/disordered nanocomposites: Hybridization and avoided crossings of localized and delocalized modes. *Advanced Functional Materials*, 28(17):1706268, feb 2018.
- [15] A. Tlili, V. M. Giordano, Y. M. Beltukov, P. Desmarchelier, S. Merabia, and A. Tanguy. Enhancement and anticipation of the ioffe–regel crossover in amorphous/nanocrystalline composites. *Nanoscale*, 11(44):21502–21512, 2019.
- [16] W Schirmacher, C Tomaras, B Schmid, G Baldi, G Vilianni, G Ruocco, and T Scopigno. Sound attenuation and anharmonic damping in solids with correlated disorder. *Condensed Matter Physics*, 2010.
- [17] Y. M. Beltukov, C. Fusco, D. A. Parshin, and A. Tanguy. Boson peak and ioffe-regel criterion in amorphous siliconlike materials: The effect of bond directionality. *Physical Review E*, 93(2):023006, feb 2016.
- [18] Simon Gelin, Hajime Tanaka, and Anaël Lemaître. Anomalous phonon scattering and elastic correlations in amorphous solids. *Nature Materials*, 15(11):1177–1181, aug 2016.
- [19] T. Damart, A. Tanguy, and D. Rodney. Theory of harmonic dissipation in disordered solids. *Physical Review B*, 95(5):054203, feb 2017.
- [20] YM Beltukov, DA Parshin, VM Giordano, and A Tanguy. Propagative and diffusive regimes of acoustic damping in bulk amorphous material. *Physical Review E*, 98(2):023005, 2018.
- [21] G. Ruocco, F. Sette, R. Di Leonardo, D. Fioretto, M. Krisch, M. Lorenzen, C. Masciovecchio, G. Monaco, F. Pignon, and T. Scopigno. Nondynamic origin of the high-frequency acoustic attenuation in glasses. *Physical Review Letters*, 83(26):5583–5586, dec 1999.

- [22] G. Baldi, V. M. Giordano, G. Monaco, and B. Ruta. Sound attenuation at terahertz frequencies and the boson peak of vitreous silica. *Physical Review Letters*, 104(19):195501, may 2010.
- [23] B. Rufflé, M. Foret, E. Courtens, R. Vacher, and G. Monaco. Observation of the onset of strong scattering on high frequency acoustic phonons in densified silica glass. *Physical Review Letters*, 90(9):095502, mar 2003.
- [24] B. Rufflé, G. Guimbretière, E. Courtens, R. Vacher, and G. Monaco. Glass-specific behavior in the damping of acousticlike vibrations. *Physical Review Letters*, 96(4):045502, jan 2006.
- [25] G. Monaco and V. M. Giordano. Breakdown of the debye approximation for the acoustic modes with nanometric wavelengths in glasses. *Proceedings of the National Academy of Sciences*, 106(10):3659–3663, feb 2009.
- [26] Hideyuki Mizuno, Giancarlo Ruocco, and Stefano Mossa. Sound damping in glasses: Interplay between anharmonicities and elastic heterogeneities. *Physical Review B*, 101(17):174206, may 2020.
- [27] S. Ayrinhac, M. Foret, A. Devos, B. Rufflé, E. Courtens, and R. Vacher. Subterahertz hypersound attenuation in silica glass studied via picosecond acoustics. *Physical Review B*, 83:014204, 2011.
- [28] René Vacher, Jacques Pelous, and Eric Courtens. Mean free path of high-frequency acoustic excitations in glasses with application to vitreous silica. *Physical Review B*, 56(2):R481–R484, jul 1997.
- [29] G. Monaco and S. Mossa. Anomalous properties of the acoustic excitations in glasses on the mesoscopic length scale. *Proceedings of the National Academy of Sciences*, 106(40):16907–16912, sep 2009.
- [30] C. Masciovecchio, A. Gessini, S. Di Fonzo, L. Comez, S. C. Santucci, and D. Fioretto. Inelastic ultraviolet scattering from high frequency acoustic modes in glasses. *Physical Review Letters*, 92(24):247401, jun 2004.
- [31] P. Benassi, S. Caponi, R. Eramo, A. Fontana, A. Giugni, M. Nardone, M. Sampoli, and G. Vilianni. Sound attenuation in a unexplored frequency region: Brillouin ultraviolet light scattering measurements in  $\text{SiO}_2$ . *Physical Review B*, 71(17):172201, may 2005.
- [32] C. Masciovecchio, G. Baldi, S. Caponi, L. Comez, S. Di Fonzo, D. Fioretto, A. Fontana, A. Gessini, S. C. Santucci, F. Sette, G. Vilianni, P. Vilmercati, and G. Ruocco. Evidence for a crossover in the frequency dependence of the acoustic attenuation in vitreous silica. *Physical Review Letters*, 97(3):035501, jul 2006.
- [33] A. Devos, M. Foret, S. Ayrinhac, P. Emery, and B. Rufflé. Hypersound damping in vitreous silica measured by picosecond acoustics. *Physical Review B*, 77(10):100201, mar 2008.

- [34] W. Dietsche and H. Kinder. Spectroscopy of phonon scattering in glass. *Physical Review Letters*, 43(19):1413–1417, nov 1979.
- [35] U. Buchenau. Evaluation of x-ray brillouin scattering data. *Physical Review E*, 90(6):062319, dec 2014.
- [36] Lijin Wang, Ludovic Berthier, Elijah Flenner, Pengfei Guan, and Grzegorz Szamel. Sound attenuation in stable glasses. *Soft Matter*, 15(35):7018–7025, 2019.
- [37] T. Scopigno, S. N. Yannopoulos, D. Th. Kastrissios, G. Monaco, E. Pontecorvo, G. Ruocco, and F. Sette. High frequency acoustic modes in vitreous beryllium fluoride probed by inelastic x-ray scattering. *The Journal of Chemical Physics*, 118(1):311–316, jan 2003.
- [38] D. Fioretto, U. Buchenau, L. Comez, A. Sokolov, C. Masciovecchio, A. Mermet, G. Ruocco, F. Sette, L. Willner, B. Frick, D. Richter, and L. Verdini. High-frequency dynamics of glass-forming polybutadiene. *Physical Review E*, 59(4):4470–4475, apr 1999.
- [39] P. Benassi, M. Krisch, C. Masciovecchio, V. Mazzacurati, G. Monaco, G. Ruocco, F. Sette, and R. Verbeni. Evidence of high frequency propagating modes in vitreous silica. *Physical Review Letters*, 77(18):3835–3838, oct 1996.
- [40] K. S. Gilroy and W. A. Phillips. An asymmetric double-well potential model for structural relaxation processes in amorphous materials. *Philosophical Magazine B*, 43(5):735–746, may 1981.
- [41] DA Parshin, HR Schober, and VL Gurevich. Vibrational instability, two-level systems, and the boson peak in glasses. *Physical Review B*, 76(6):064206, 2007.
- [42] U. Buchenau, Yu.M. Galperin, V.L. Gurevich, D.A. Parshin, M.A. Ramos, and H.R. Schober. Interaction of soft modes and sound waves in glasses. *Physical Review B*, 46(5):2798, 1992.
- [43] Wencheng Ji, Marko Popović, Tom W. J. de Geus, Edan Lerner, and Matthieu Wyart. Theory for the density of interacting quasilocalized modes in amorphous solids. *Physical Review E*, 99:023003, 2019.
- [44] Geert Kapteijns, David Richard, and Edan Lerner. Nonlinear quasilocalized excitations in glasses: True representatives of soft spots. *Physical Review E*, 101(3):032130, mar 2020.
- [45] A. Tanguy, B. Mantisi, and M. Tsamados. Vibrational modes as a predictor for plasticity in a model glass. *Europhysics Letters*, 90(1):16004, 2010.
- [46] B. Rufflé, D. A. Parshin, E. Courtens, and R. Vacher. Boson peak and its relation to acoustic attenuation in glasses. *Physical Review Letters*, 100(1):015501, jan 2008.

- [47] C. Levelut, R. Le Parc, and J. Pelous. Dynamic sound attenuation at hypersonic frequencies in silica glass. *Physical Review B*, 73(5):052202, feb 2006.
- [48] Eugène Duval and Alain Mermet. Inelastic x-ray scattering from nonpropagating vibrational modes in glasses. *Physical Review B*, 58(13):8159–8162, oct 1998.
- [49] H. Mizuno, S. Mossa, and J.-L. Barrat. Acoustic excitations and elastic heterogeneities in disordered solids. *Proceedings of the National Academy of Sciences*, 111(33):11949–11954, aug 2014.
- [50] A. Tanguy, J.P. Wittmer, F. Leonforte, and J.-L. Barrat. Continuum limit of amorphous elastic bodies: A finite-size study of low-frequency harmonic vibrations. *Physical Review B*, 66:174205, 2002.
- [51] F. Leonforte, A. Tanguy, and J.-L. Barrat. Inhomogeneous elastic response of silica glass. *Physical Review Letters*, 97(5):055501, 2006.
- [52] Alessia Marruzzo, Walter Schirmacher, Andrea Fratallocchi, and Giancarlo Ruocco. Heterogeneous shear elasticity of glasses: the origin of the boson peak. *Scientific Reports*, 3(1):1–7, mar 2013.
- [53] Walter Schirmacher, Tullio Scopigno, and Giancarlo Ruocco. Theory of vibrational anomalies in glasses. *Journal of Non-Crystalline Solids*, 407:133–140, jan 2015.
- [54] DA Conyuh and YM Beltukov. Ioffe-regel criterion and viscoelastic properties of amorphous solids. *arXiv preprint arXiv:2012.15719*, 2020.
- [55] Philip B. Allen, Joseph L. Feldman, Jaroslav Fabian, and Frederick Wooten. Diffusons, locons and propagons: Character of atomic vibrations in amorphous si. *Philosophical Magazine B*, 79(11-12):1715–1731, nov 1999.
- [56] S. E. Skipetrov and Y. M. Beltukov. Anderson transition for elastic waves in three dimensions. *Physical Review B*, 98(6):064206, aug 2018.
- [57] John Page, Anatoliy Strybulevych, Hefei Hu, Sergey Skipetrov, and Bart van Tiggelen. Anderson localization of ultrasonic waves in three dimensions. *The Journal of the Acoustical Society of America*, 126(4):2273, 2009.
- [58] George Gabriel Stokes. On the theories of the internal friction of fluids in motion, and of the equilibrium and motion of elastic solids. In *Mathematical and Physical Papers vol.1*, pages 75–129. Cambridge University Press, 1880.
- [59] Robert O. Pohl, Xiao Liu, and EunJoo Thompson. Low-temperature thermal conductivity and acoustic attenuation in amorphous solids. *Reviews of Modern Physics*, 74(4):991–1013, oct 2002.
- [60] Walter Schirmacher. The boson peak. *physica status solidi (b)*, 250(5):937–943, feb 2013.

- [61] S Parke. Logarithmic decrements at high damping. *British Journal of Applied Physics*, 17(2):271, 1966.
- [62] Monica Carfagni, Edoardo Lenzi, and Marco Pierini. The loss factor as a measure of mechanical damping. In *Proceedings-spie the international society for optical engineering*, volume 1, pages 580–284. SPIE INTERNATIONAL SOCIETY FOR OPTICAL, 1998.
- [63] Sow-Hsin Chen and Sidney Yip. *Spectroscopy in Biology and Chemistry: Neutron, X-Ray, Laser*. Academic Press, 2017.
- [64] H. Luo, A. Gravouil, V. M. Giordano, W. Schirmacher, and A. Tanguy. Continuum constitutive laws to describe acoustic attenuation in glasses. *Physical Review E*, 102(3):033003, sep 2020.
- [65] R.C. Zeller and R.O. Pohl. Thermal conductivity and specific heat of non-crystalline solids. *Physical Review B*, 4(6):2029, sep 1971.
- [66] R.O. Pohl. Amorphous materials: Thermal conductivity. In *Encyclopedia of Materials: Science and Technology*, pages 232–237. Elsevier, 2001.
- [67] Michel Tsamados, Anne Tanguy, Chay Goldenberg, and Jean-Louis Barrat. Local elasticity map and plasticity in a model lennard-jones glass. *Physical Review E*, 80(2):026112, aug 2009.
- [68] Haoming Luo, Anthony Gravouil, Valentina Giordano, and Anne Tanguy. Thermal transport in a 2d nanophononic solid: Role of bi-phasic materials properties on acoustic attenuation and thermal diffusivity. *Nanomaterials*, 9(10):1471, oct 2019.
- [69] R. Vacher, H. Sussner, and S. Hunklinger. Brillouin scattering in vitreous silica below 1 k. *Physical Review B*, 21(12):5850–5853, jun 1980.